科学通报 2024 年 第 69 卷 第 18 期: 2602 ~ 2617
中山大学地球科学学科(地质学)创立100周年专辑 论 文
《中国科学》杂志社 SCIENCE CHINA PRESS

粤西高州泥质麻粒岩变质*P-T-t*演化及其对华南早古生代构造背景的指示

钱加慧[1*], 梁勇智[1], 尹常青[1], 高彭[1], 张健[2], 热孜亚·麦麦提[1]

1. 中山大学地球科学与工程学院, 广东省地质过程与矿产资源探查重点实验室, 珠海 519080;
2. 香港大学地球科学系, 香港 999077
* 联系人, E-mail: qianjh5@mail.sysu.edu.cn

2023-08-13 收稿, 2023-09-27 修回, 2023-10-28 接受, 2023-11-02 网络版发表
国家自然科学基金(42325205, 42372227, 41972197, 42025204)和广东省基础与应用基础研究基金(2024A1515010771, 2019A1515012189)资助

摘要 华南陆块早古生代构造热事件的形成与演化一直是学界关注的热点议题. 本文对地处华夏地块西南部的高州泥质麻粒岩开展了详细的岩相学、矿物化学、相平衡模拟和锆石年代学研究, 综合华夏地块已有的早古生代变质作用资料, 探讨了华南早古生代时期的构造背景. 高州泥质麻粒岩包含三阶段矿物组合: 包裹体组合由石榴子石核部及所包裹的钾长石、黑云母、矽线石、石英、金红石和钛铁矿组成, 相平衡模拟获得温压条件为~0.95 GPa/800°C(压力峰期阶段); 基质矿物组合为石榴子石变斑晶和基质中的堇青石、钾长石、黑云母、石英、矽线石和钛铁矿, 结合矿物组合在相图中的位置、基质黑云母的Ti含量和基质钾长石的Ab值, 限定温压条件为0.57~0.69 GPa/815~865°C(温度峰期阶段); 退变质组合以石榴子石周围或后成合晶中的堇青石、钾长石、黑云母、石英和钛铁矿以及晚期斜长石和矽线石为代表, 指示降温降压的退变质过程. 高州泥质麻粒岩的锆石U-Pb定年获得441±1.4 Ma的变质年龄. 变质锆石的Ti温度计计算结果为693~759°C, 与岩石的退变质冷却温度一致. 华南早古生代变质作用整体上为中压相系条件, 变质*P-T*轨迹均为顺时针样式, 暂无高压相系蓝片岩或榴辉岩的发现. 上述变质作用特征在大陆碰撞造山带和陆内造山带都可形成, 但碰撞造山带的另一个特点是常伴生高压-超高压蓝片岩和榴辉岩. 从目前掌握的变质作用数据和其他地质资料分析, 华南陆块内部发育早古生代变质-岩浆-变形作用的构造域很可能并不是发生俯冲-碰撞的"第一现场", 引起该期构造热事件的应力来源于彼时华南的陆缘.

关键词 泥质麻粒岩, 变质*P-T-t*演化, 早古生代, 构造意义, 华南

华南陆块主要由扬子地块和华夏地块组成(图1(a)), 其北缘以秦岭-大别-苏鲁造山带与华北克拉通分隔, 西北以龙门山-横断山断裂带为界, 与松潘-甘孜地体相接, 西南缘以哀牢山-红河断裂带与印支陆块相隔, 东南侧为西太平洋构造域[2~4]. 多数学者认为, 扬子地块和华夏地块在新元古代早期(晋宁期)沿华南中部(江南造山带)碰撞拼合, 形成统一的华南陆块, 此后华南陆块经历了南华纪裂解和从扬子地块到华夏地块连续一致的地层沉积与生态演化, 以及早古生代时期的大规模构造-变质-岩浆作用, 形成了早古生代陆内造山带(图1(b))[2,5~10]. 该陆内造山带并非直接由汇聚板块间的碰撞作用产生, 而是由华南外围陆缘与未知陆块发生俯冲-碰撞所引起的应力远程传导至华南大陆内部所产生[5~8,11]. 华南早古生代陆内造山作用与欧洲加里东造山运动的时代相同, 因此也被称为华南加里东造山带(褶皱带)[6], 亦或被称为广西造山运动[2]、武夷-云开

引用格式: 钱加慧, 梁勇智, 尹常青, 等. 粤西高州泥质麻粒岩变质*P-T-t*演化及其对华南早古生代构造背景的指示. 科学通报, 2024, 69: 2602–2617
Qian J H, Liang Y Z, Yin C Q, et al. Metamorphic *P-T-t* evolution of pelitic granulite from Gaozhou, western Guangdong Province and its implications for the Early Paleozoic tectonic setting in South China (in Chinese). Chin Sci Bull, 2024, 69: 2602–2617, doi: 10.1360/TB-2023-0835

© 2023《中国科学》杂志社

造山带[7], 其影响范围主要为扬子地块东缘和华夏地块的政和-大埔断裂以西部分(图1(a)).

过去20年, 前人在华夏地块陆续发现了早古生代高级变质岩石, 如浙江陈蔡地区的泥质和基性麻粒岩[12]、浙江龙游地区的榴闪岩及其围岩副片麻岩[13,14]、赣东北周潭地区的基性麻粒岩[15]、南岭桃溪地区的泥质麻粒岩[16,17]、粤西高州地区的泥质-半泥质麻粒岩[18]和钙硅酸盐麻粒岩[19], 以及海南岛中部的基性麻粒岩[17]. 一些学者通过这些高级变质岩石的变质作用研究, 对华南早古生代构造热事件的动力学机制提出了不同的观点. 例如, 陈相艳等人[13]认为龙游榴闪岩具有退变榴辉岩特征, 峰期达到高压相系榴辉岩相条件. 由于高压相系变质是反映汇聚板块边缘俯冲-碰撞过程的强有力证据, 因此他们推测华夏地块在早古生代曾发生俯冲-碰撞造山事件[13]. 这一发现引起了学界的广泛关注和接续研究, 但遗憾的是, 后续的工作均未在龙游榴闪岩中发现确凿的榴辉岩相或由榴辉岩相退变形成的矿物学记录, 其峰期条件应为中压相系的麻粒岩相[20~22]. 仝来喜课题组[14,18,19]在高州麻粒岩和龙游副片麻岩的变质作用研究基础上, 总结华夏地块早古生代变质*P-T*轨迹以顺时针样式为特征, 形成于俯冲-碰撞构造环境, 记录了扬子地块与华夏地块陆-陆碰撞及碰撞后抬升的演化过程. 一般来说, 具有顺时针型*P-T*轨迹的中压相系变质作用, 可以反映存在一定程度的地壳加厚, 但其成因具有多解性, 既可以通过俯冲-碰撞过程形成, 也能在陆内造山环境下产生[23~25]. 此外, 关于华南是否存在早古生代时期与俯冲-碰撞相关的蛇绿岩组合或者典型岛弧岩浆岩组合等科学问题, 学界也存在巨大争议[2,3,26~31], 因此尚需更多工作去探讨早古生代构造热事件的动力学过程.

新近, 许多学者从构造地质学、岩浆作用、岩石圈结构、古地磁和古生物地层等不同视角对华南早古生代构造演化过程提出了新的解释. (1) Lin等人[4]通过详细的构造解析提出华南的早古生代大洋存在于华夏地块东部, 华夏地块位于俯冲和碰撞造山带的下盘, 早古生代蛇绿岩和弧岩浆位于(某未知的)上盘板块, 该上

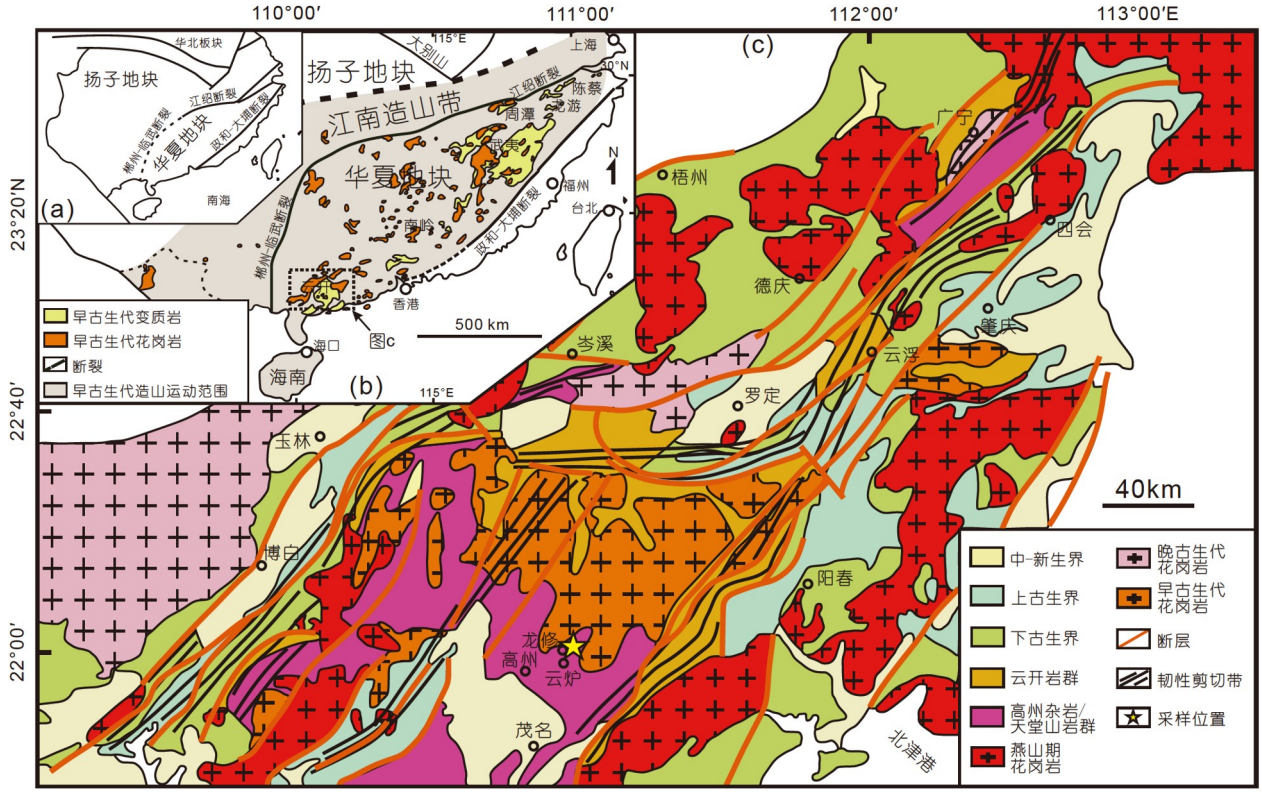

图 1 华夏地块云开地区地质简图. (a) 华南陆块构造划分方式, 据文献[1]修改; (b) 华南早古生代造山运动范围与该期变质岩和花岗岩分布位置, 据文献[1,7]修改; (c) 云开地区地质体组成与接触关系, 引自文献[36]

Figure 1 Simplified geological map of the Yunkai area, Cathaysia Block. (a) Tectonic division of South China, modified from Ref. [1]; (b) range of the early Paleozoic orogeny in South China and distribution of the early Paleozoic metamorphic rocks and granites, modified from Refs. [1,7]; (c) geological constituents and their contacting relationships in the Yunkai area, cited from Ref. [36]

盘板块在碰撞后走滑游离，从而导致华南内部缺少早古生代蛇绿岩等代表大洋的直接地质记录. (2) 黄小龙和于洋[10]对华南不同区域早古生代花岗岩和基性岩的分布规律、成因变化、地质意义等作了系统梳理，指出华南早古生代构造热事件既有俯冲-碰撞的特征，又兼具陆内造山的属性，因而针对性地建立了华夏地块与某一未知块体俯冲-碰撞(沿现今政和-大埔断裂带位置)、华夏与扬子的结合部位(新元古代江南造山带位置)发生陆内挤压的陆内-碰撞复合型造山模型. (3) Zhao等人[31]强调东华夏地块和西华夏地块具有明显不同的岩石圈结构且在政和-大埔断裂之下存在两个不同的板片[32]，提出了东、西华夏地块之间的洋-陆碰撞模型，其中东华夏地块从古生代时期的大洋岩石圈发展而来，存在西华夏地块大陆地壳物质向东华夏地块的逆冲推覆，碰撞作用的发生受到冈瓦纳大陆拼合过程的远程应力驱动. (4) Wang等人[33]综合了扬子地块和华夏地块的古地磁、古生物、地层学和碎屑锆石资料，认为扬子地块和华夏地块直到早古生代晚期才通过走滑运动或斜向碰撞并置在一起, 在此之前, 两者位于冈瓦纳大陆北缘的两个不同部位. 由此可见, 学界一直在持续地探索华南早古生代构造背景，并在岩浆作用、沉积地层和构造-地球物理等方面积累了丰富的资料, 但变质作用的研究则相对较为零散, 从整体变质演化的视角对构造过程的讨论仍不够充分.

麻粒岩是构成大陆下地壳的主要岩石类型，是研究下地壳物质成分和演化的重要窗口，同时也是造山带的重要组成部分，可以有效揭示造山带的构造热演化过程, 因此麻粒岩受到广泛关注[34]. 粤西高州杂岩中的泥质麻粒岩包含典型麻粒岩相矿物组合，宏观上和微观上的变质反应结构、熔融结构均很清楚，是开展变质-深熔分析、恢复变质历史的理想载体. 本文在前人研究的基础上，对高州泥质麻粒岩开展系统的岩石学、变质相平衡模拟和年代学研究，详细刻画岩石的变质*P-T-t*轨迹, 并综合华南早古生代变质作用特征, 探讨地球动力学机制. 本文使用的矿物缩写参考国际矿物学会-新矿物命名及分类委员会最新推荐的矿物代号[35], 熔体用L表示.

1 研究区地质概况

云开地体位于华夏地块的西南部，粤西和桂东南的交界地区，呈南西-北东向展布(图1(b)). 云开地体总出露面积约50000 km^2, 传统上认为其被东部的吴川-四会断裂带、西部的岑溪-博白断裂带以及北部的罗定-广宁断裂带所围限[36]，是华南早古生代造山带的重要组成部分(图1(c)). 云开地体主要由以高州杂岩(也被称为天堂山岩群)与云开岩群为代表的变质基底和各类不同时代的花岗质岩石组成，出露少量中-新生代沉积盖层. 高州杂岩位于云开地体的腹地, 由经历了角闪岩相-麻粒岩相(中-高级)变质的火山-碎屑沉积岩组成, 岩石类型包括副片麻岩、片岩、石英岩、大理岩和各类(泥质、半泥质、钙硅酸盐型)麻粒岩, 它们的原岩主要形成于中-新元古代，变质年龄为早古生代加里东期和中生代印支期[18,19,36]. 高州杂岩内部及周边出露大量早古生代到中生代花岗岩，外围地质体的岩石物质组成和碎屑锆石年龄谱均与高州杂岩非常相似，但仅经历了中-低级变质作用, 称为云开岩群[36].

本研究区位于粤西高州东部的龙修-云炉一带(图1(c)), 区内整体变质级别较高, 可观察到混合岩化现象, 泥质麻粒岩呈透镜体样式，与片麻状花岗岩共生或以包体形式产于紫苏花岗岩中[18]. 陈斌和庄育勋[37]曾描述这些泥质麻粒岩的矿物化学特征，推测岩石形成在高fCO$_2$、低fH$_2$O的环境中. Li等人[18]在泥质麻粒岩中识别出斜方辉石和尖晶石，认为岩石经历了低压-高温的峰期变质作用, 峰期后以近等压降温为特征. 这一结果与李超等人[19]在高州钙硅酸盐麻粒岩中获得的温压条件和*P-T*轨迹一致, 但与华南其他地区以中-高压峰期变质、近等温降压为主的早古生代变质特征不同[13~17,22]. 锆石U-Pb年代学研究表明高州地区麻粒岩相变质作用发生于435~445 Ma[18,19]. 紫苏花岗岩的侵位时代约为431 Ma，表明紫苏花岗岩的成因与区域上的早古生代麻粒岩相变质作用有密切关联，可能形成于造山后抬升过程[38].

2 样品特征

高州泥质麻粒岩样品(G2014)采自高州水库以南3 km、高州龙修村东侧的灯心垌附近(22°0′35.76″N, 111°3′34.08″E), 其围岩为黑云斜长片麻岩(片麻状花岗岩, 图S1). 泥质麻粒岩表面受到少许风化, 新鲜面呈深灰色, 可见不同尺度的长英质细脉, 指示岩石曾发生部分熔融. 岩石具有块状构造, 斑状变晶结构, 变斑晶为肉红色的石榴子石(图2(a)和S2). 岩石的主要矿物组成包括：石榴子石8vol%~10vol%(图S3)、钾长石约20vol%~22vol%、堇青石18vol%~20vol%、黑云母约15vol%、石英20vol%~22vol%、斜长石3vol%~5vol%、

矽线石3vol%~5vol%，以及少量副矿物钛铁矿、金红石、黄铁矿和磷灰石等(图2(b)~(d)和3). 一般来说, 黄铁矿和磷灰石含有挥发性成分，在恢复变质条件时的作用不大，因此在以下论述中暂不考虑这两种矿物[22].

石榴子石变斑晶粒径为0.5~1.5 mm, 可见港湾状分解边，内部含有钾长石、黑云母、矽线石、金红石、钛铁矿和浑圆状石英等包裹体，形成筛状结构(图2(b)和3(a), (b)). 部分石榴子石分解较为明显，仅留下一点残余(图2(c)). 钾长石主要以半自形板状分布于基质中, 少量钾长石以石榴子石包裹体出现或与黑云母、堇青石构成晚期的后成合晶(图2(b)). 堇青石有两类: 第一类堇青石位于基质中，与基质钾长石、黑云母和石英等矿物平衡共生，有时包含钛铁矿或黑云母等矿物(图2(d)和3(c), (d)); 另一类堇青石呈“它”形生长在石榴子石变斑晶周边或以后成合晶的形式出现(图2(b), (c)), 应形成于晚期退变质阶段. 黑云母为棕色, 结构上可分为3类: 第一类为石榴子石或基质堇青石中的包裹体; 第二类以片状形式出现在基质中(图2(d)); 第三类紧邻或围绕石榴子石及其他基质矿物，或发生分解并与钾长石和堇青石构成后成合晶(图2(b), (c)), 表明该类黑云母形成于晚期退变质过程. 矽线石和石英在石榴子石的包裹体中、基质中和晚期结构域中均有出现. 斜长石为浑圆细粒状或不规则条带状，从结构上初步区分为包裹体型(石榴子石中)和晚期型(分布于基质矿物的间隙)(图2(c)). 需要指出的是: (1) 包裹体斜长石均位于石榴子石边缘裂隙或凹口处, 根据经验判断, 这些斜长石很可能仅是形态上像“包裹体”，实际应该属于晚期生长，这一推测也得到了斜长石An值(0.66~0.82，与晚期斜长石的富钙部分相似)的支持; (2) 晚期斜长石很多呈“薄膜”样形态(图3(c))，可能代表了熔体结晶的产物. 金红石均为石榴子石包裹体，与钛铁矿共生(图3(a)). 钛铁矿在各个结构域中均存在.

根据上述观察到的岩相学特征，高州泥质麻粒岩样品可划分出3个阶段矿物组合: (1) 包裹体矿物组合, 主要包括石榴子石核部及所包裹的钾长石、黑云母、矽线石、石英、金红石和钛铁矿; (2) 基质矿物组合, 包括石榴子石变斑晶和基质中的堇青石、钾长石、黑云母、矽线石、石英和钛铁矿; (3) 退变质矿物组合, 主要为石榴子石周围或后成合晶中的堇青石、钾长石、黑云母、石英和钛铁矿，以及晚期斜长石和晚期矽线石等.

3 实验方法与分析结果

3.1 矿物化学

利用中山大学地球科学与工程学院物质成分分析实验室SHIMADZU-1720HT型电子探针对矿物化学成分和背散射图像进行分析. 仪器测试条件: 加速电压为15 kV, 电子束流为20 nA, 束斑为1~5 μm. 采用美国SPI公司的53种天然矿物和合成矿物进行标准化，分析结果的相对误差小于2%.

高州泥质麻粒岩样品的石榴子石显示了从核到边的成分变化(图4(a)). 其中，铁铝榴石(X_{Alm}=Fe^{2+}/(Fe^{2+}+Mg+Ca+Mn)；其他三类端元的计算方式相似)含量较高，整体上从核部(C)向边部(R1和R2)增大(0.78→0.85)；镁铝榴石(X_{Prp})含量从核部向边部减小(0.17→0.09)，表明石榴子石成分发生了扩散[39]；钙铝榴石(X_{Grs})和锰铝榴石(X_{Sps})含量均很低，分别为0.04左右和0.01~0.02(表1). 基质堇青石比晚期堇青石略贫铁，两者的X_{Fe}(=Fe^{2+}/(Fe^{2+}+Mg))值分别为0.35~0.37和0.37~0.42. 基质钾长石的钠质端元Ab(=Na/(Ca+Na+K))值(0.13~0.16)低于晚期阶段的钾长石Ab值(0.30~0.34). 不同产状黑云母的成分有差异，包裹体、基质和晚期黑云母的X_{Mg}(=Mg/(Fe^{2+}+Mg))值分别为0.38~0.49、0.40~0.41和0.37~0.41，基质黑云母的Ti含量最高，为0.20~0.27，包裹体和晚期黑云母的Ti含量分别为0.14~0.20和0.16~0.22(图4(b)). Li等人[18]也在高州泥质麻粒岩中测到了高Ti值(0.25)的基质黑云母. 斜长石的牌号An(=Ca/(Ca+Na+K))值变化范围较大，“包裹体”斜长石的An值为0.66~0.82，晚期斜长石的An值变化于0.23~0.82(图4(c), 表1).

3.2 变质相平衡模拟

在岩相学观察和矿物化学成分分析的基础上，本文采用THERMOCALC 3.40程序和ds62热力学数据库[40]对高州泥质麻粒岩样品(G2014)进行相平衡模拟. 选择的模式体系为NCKFMASHTO(Na_2O-CaO-K_2O-FeO-MgO-Al_2O_3-SiO_2-H_2O-TiO_2-O)，石英设为过量，MnO在全岩和各矿物中的含量很低，忽略不计. 假设P全部在磷灰石中，扣除P_2O_5的同时也相应扣减了CaO. 水值和氧值分别通过前期计算的T-H_2O图和T-O图确定, 最后用于P-T视剖面图计算的全岩成分见图后说明. 相平衡模拟采用的矿物活度模型为: 熔体、石榴子石、黑云母、斜方辉石和堇青石[41]，斜长石和钾长

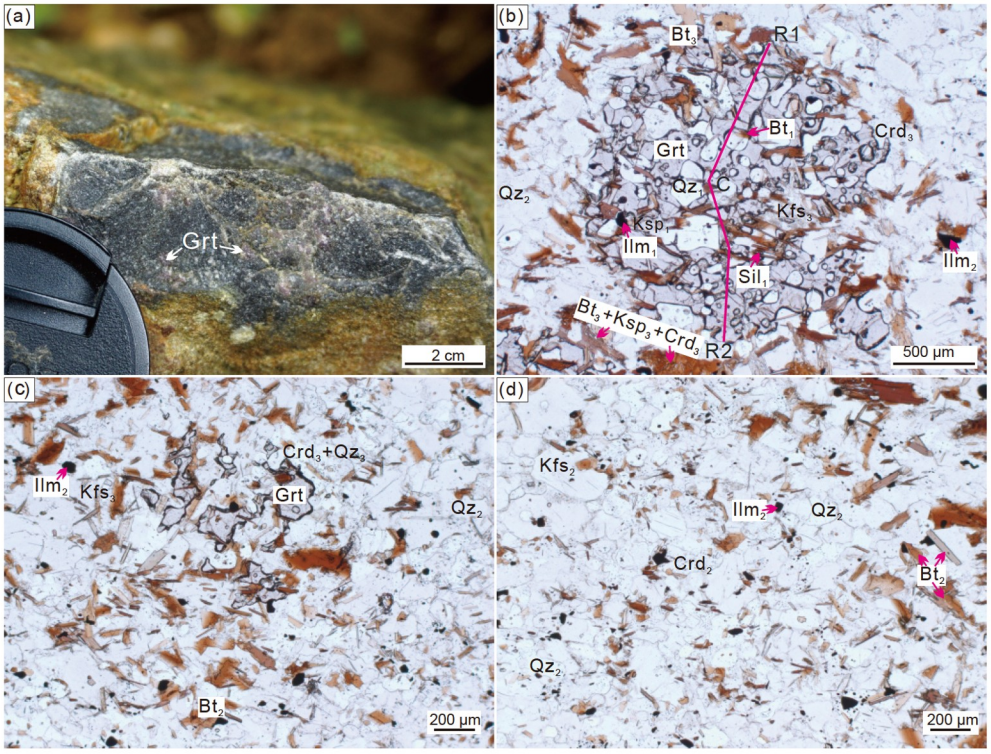

图 2 高州泥质麻粒岩露头照片(a)与单偏光镜下显微结构特征(b)~(d)
Figure 2 Outcrop photo (a) and microstructures (b)−(d) of pelitic granulite from Gaozhou under plane-polarized light

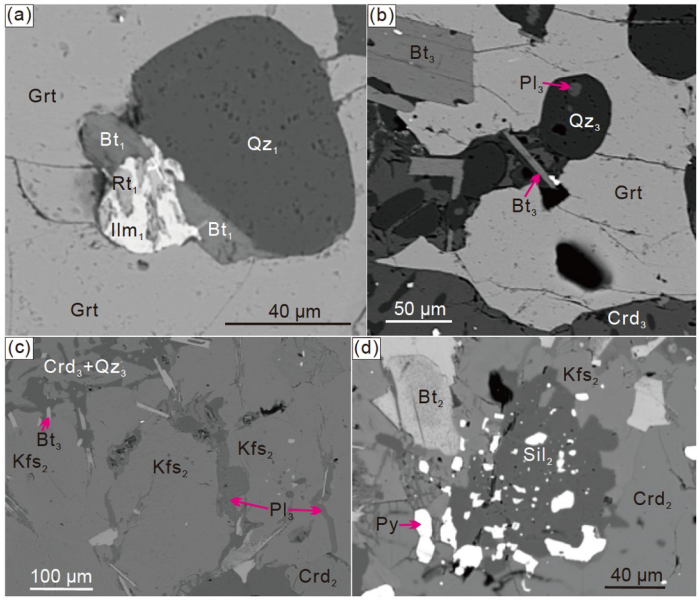

图 3 高州泥质麻粒岩背散射显微照片. (a) 石榴子石中的矿物包裹体; (b) 石榴子石的港湾状边; (c), (d) 基质矿物与退变质矿物特征
Figure 3 Back-scattered electron micrographs of pelitic granulite from Gaozhou. (a) Mineral inclusions in garnet; (b) embayed rim of garnet; (c), (d) characteristics of the matrix minerals and retrograde minerals

石[42], 钛铁矿和磁铁矿[43], 尖晶石[44], 蓝晶石、矽线石、金红石和石英为纯端元组分.

高州泥质麻粒岩的*P*-*T*视剖面图在0.30~1.10 GPa/650~900°C条件下计算(图5(a)). 固相线出现在710~

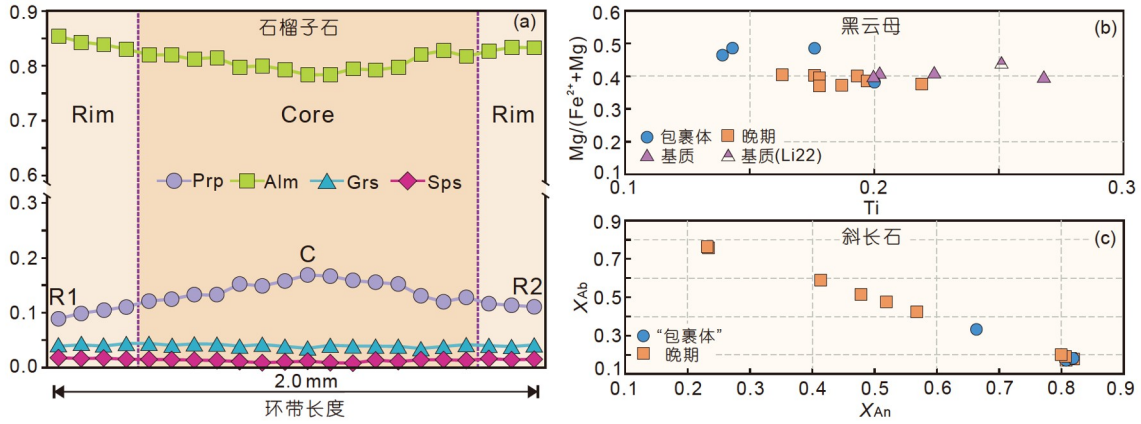

图 4 高州泥质麻粒岩石榴子石成分(a)、黑云母成分(b)与斜长石成分(c). 数据"Li22"引自文献[18]

Figure 4 Chemical compositions of garnet (a), biotite (b) and plagioclase (c) in pelitic granulite from Gaozhou. "Li22" is cited from Ref. [18]

表 1 高州泥质麻粒岩样品的电子探针分析结果[a)]

Table 1 Microprobe analyses for pelitic granulite sample from Gaozhou

矿物	Grt-C	Grt-R1	Crd-基质	Crd-晚期	Kfs-包裹体	Kfs-基质	Kfs-晚期	Bt-包裹体	Bt-基质	Bt-晚期	Pl-"包裹体"	Pl-晚期
SiO_2	36.63	36.88	46.55	47.55	64.51	63.83	63.91	32.34	36.98	37.20	50.92	52.76
TiO_2	0.04	0.07	0.00	0.03	0.03	0.00	0.08	3.42	4.82	2.88	0.00	0.05
Al_2O_3	20.76	20.11	31.10	30.47	19.00	18.52	18.51	19.00	18.94	19.52	30.62	28.43
Cr_2O_3	0.11	0.14	0.00	0.00	0.00	0.02	0.05	0.27	0.06	0.03	0.00	0.00
Fe_2O_3	1.75	0.43	2.19	2.36	1.33	0.10	0.10	0.01	0.00	0.00	0.60	0.10
FeO	34.23	39.36	7.87	8.48	0.00	0.00	0.02	22.03	19.95	19.51	0.00	0.00
MnO	0.50	0.80	0.04	0.02	0.00	0.02	0.02	0.04	0.02	0.00	0.04	0.00
MgO	4.15	2.29	8.19	7.84	0.00	0.02	0.00	7.61	7.43	7.45	0.00	0.00
CaO	1.20	1.40	0.03	0.02	0.00	0.00	0.00	0.00	0.00	0.00	14.36	11.00
Na_2O	0.04	0.06	0.43	0.34	1.54	1.75	3.83	0.24	0.17	0.21	3.97	6.56
K_2O	0.00	0.00	0.01	0.02	13.63	14.11	13.77	8.52	8.91	8.57	0.08	0.10
总量	99.41	101.54	96.41	97.13	100.04	98.37	100.29	93.48	97.28	95.37	100.59	99.00
O	12.00	12.00	18.00	18.00	8.00	8.00	8.00	11.00	11.00	11.00	8.00	8.00
Si	2.96	2.98	4.93	5.01	2.96	2.98	2.95	2.56	2.74	2.80	2.32	2.42
Ti	0.00	0.00	0.00	0.00	0.00	0.00	0.00	0.20	0.27	0.16	0.00	0.00
Al	1.98	1.91	3.89	3.79	1.03	1.02	1.01	1.77	1.66	1.73	1.64	1.54
Cr	0.01	0.01	0.00	0.00	0.00	0.00	0.00	0.02	0.00	0.00	0.00	0.00
Fe^{3+}	0.11	0.03	0.17	0.19	0.05	0.00	0.00	0.00	0.00	0.00	0.02	0.00
Fe^{2+}	2.31	2.66	0.70	0.75	0.00	0.00	0.00	1.46	1.24	1.23	0.00	0.00
Mn	0.03	0.06	0.00	0.00	0.00	0.00	0.00	0.00	0.00	0.00	0.00	0.00
Mg	0.50	0.28	1.29	1.23	0.00	0.00	0.00	0.90	0.82	0.84	0.00	0.00
Ca	0.10	0.12	0.00	0.00	0.00	0.00	0.00	0.00	0.00	0.00	0.70	0.54
Na	0.01	0.01	0.09	0.07	0.14	0.16	0.34	0.04	0.02	0.03	0.35	0.59
K	0.00	0.00	0.00	0.00	0.80	0.84	0.81	0.86	0.84	0.82	0.00	0.01
X(矿物)	0.04	0.04	0.35	0.38	0.15	0.16	0.30	0.38	0.40	0.41	0.66	0.48

a) $X(\mathrm{Grt})=X_{\mathrm{Grs}}=\mathrm{Ca}/(\mathrm{Ca}+\mathrm{Mg}+\mathrm{Fe}^{2+})$; $X(\mathrm{Crd})=X_{\mathrm{Fe}}=\mathrm{Fe}^{2+}/(\mathrm{Fe}^{2+}+\mathrm{Mg})$; $X(\mathrm{Kfs})=\mathrm{Ab}=\mathrm{Na}/(\mathrm{Na}+\mathrm{Ca}+\mathrm{K})$; $X(\mathrm{Bt})=X_{\mathrm{Mg}}=\mathrm{Mg}/(\mathrm{Fe}^{2+}+\mathrm{Mg})$; $X(\mathrm{Pl})=\mathrm{An}=\mathrm{Ca}/(\mathrm{Na}+\mathrm{Ca}+\mathrm{K})$. C、R1对应图2(b)和4(a)的编号位置

790°C的位置, 金红石稳定于0.75 GPa以上, 堇青石在低压部分出现. 图5(a)计算了石榴子石(忽略Mn)的X_{Grs}(=Ca/(Fe^{2+}+Mg+Ca))、黑云母的Ti、堇青石的X_{Fe}、钾长石的Ab和斜长石的An等值线. 岩相学观察到的包裹体矿物组合(Grt+Kfs+Bt+Sil+Qz+Rt+Ilm+(L))位于0.75~1.03 GPa/780~890°C的温压范围, 其中金红石的出现线指示了压力条件的下限; 再结合包裹体黑云母Ti的最大值(0.20)以及石榴子石核部X_{Grs}值(0.04), 获得温压条件为0.91~0.94 GPa/780~795°C, 代表压力峰期阶段. 基质矿物组合(Grt+Crd+Kfs+Bt+Sil+Qz+Ilm+(L))稳定在0.46~0.74 GPa/775~890°C的区域; 利用基质黑云母Ti含量(0.20~0.27)和基质钾长石的Ab值(0.13~0.16)进一步将温压条件限定为0.57~0.69 GPa/815~865°C, 代表温度峰期阶段. 从压力峰期阶段到温度峰期阶段, 发生降压并伴随升温, 这个过程与金红石消失、黑云母Ti含量升高的现象一致, 石榴子石的含量在此期间增多, 堇青石在温度峰期阶段快速形成(图S4). 晚期矿物组合以石榴子石周围或后成合晶中生长堇青石、钾长石和黑云母等为特征, 晚期斜长石呈"它"形条带状分布于基质矿物间隙, 指示石榴子石分解的退变质过程; 堇青石的X_{Fe}(0.37~0.42)、斜长石的An值和黑云母Ti的最小值(0.16)表明退变质*P-T*轨迹以降温降压为特征(图5(a)).

岩石从压力峰期阶段到温度峰期阶段存在较明显的减压-升温熔融作用(图S4), 熔融产生的熔体会发生不同程度的迁移, 从而使麻粒岩残留体具有与早期变质阶段不同的全岩成分[45]. 为了更好地限定压力峰期阶段的温压条件, 本文开展了熔体回算工作. 采用田作林等人[45]推荐的方法, 先通过实测全岩成分计算的*P-T*视剖面图确定需要加回的熔体成分以及含量, 然后

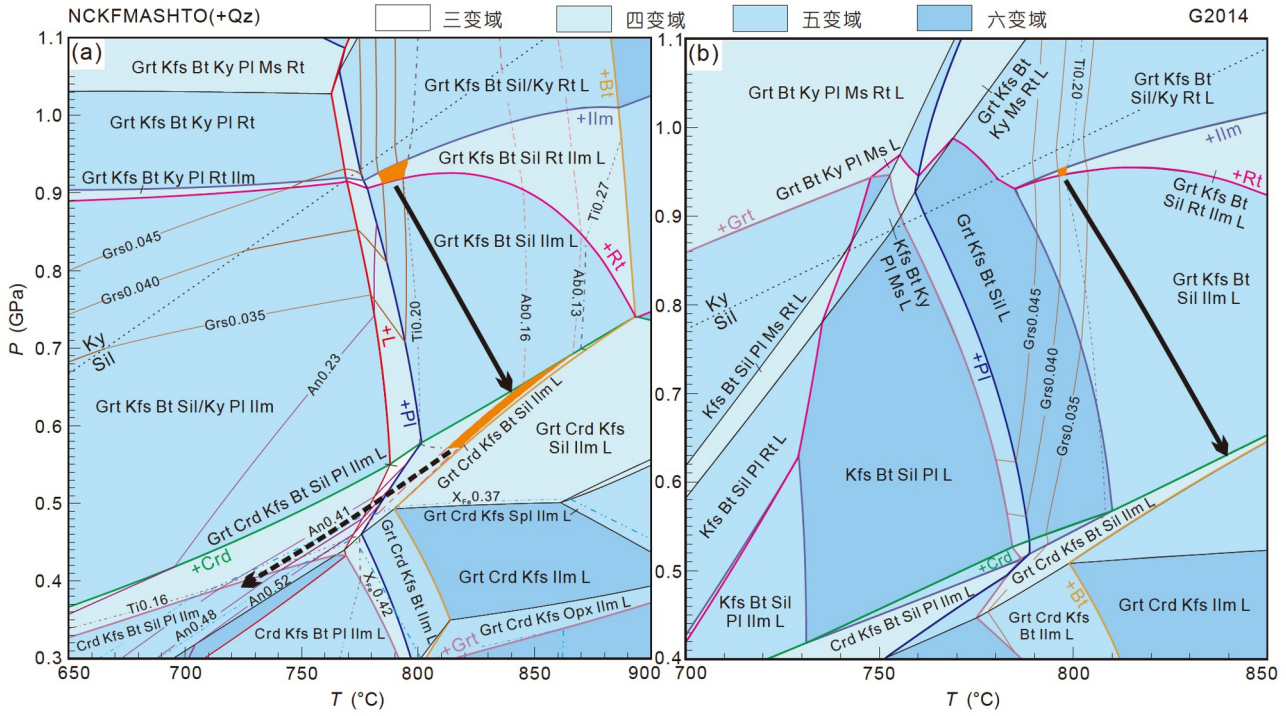

图 5 高州泥质麻粒岩*P-T*视剖面图. (a) 利用实测全岩成分(质量百分数比): SiO_2=60.89%, TiO_2=0.98%, Al_2O_3=20.41%, TFe_2O_3=7.92%, MgO=3.66%, CaO=0.25%, Na_2O=0.50%, K_2O=4.35%, P_2O_5=0.08%和*T*-H_2O(O)图确定的水值和氧值进行计算, 摩尔比值为: SiO_2=66.35%, TiO_2=0.80%, Al_2O_3=13.11%, FeO=6.50%, MgO=5.95%, CaO=0.17%, Na_2O=0.53%, K_2O=3.02%, H_2O=3.40%, O=0.17%. (b) 利用熔体回算后的有效全岩成分计算, 摩尔比值为: SiO_2=65.60%, TiO_2=0.60%, Al_2O_3=11.64%, FeO=4.99%, MgO=4.49%, CaO=0.22%, Na_2O=0.82%, K_2O=3.30%, H_2O=8.21%, O=0.13%. 等值线为石榴子石的X_{Grs}、黑云母的Ti、堇青石的X_{Fe}、钾长石的Ab和斜长石的An

Figure 5 *P-T* pseudosections of pelitic granulite from Gaozhou. (a) The bulk-rock compositions are those analysed results (mass percents: SiO_2=60.89%, TiO_2=0.98%, Al_2O_3=20.41%, TFe_2O_3=7.92%, MgO=3.66%, CaO=0.25%, Na_2O=0.50%, K_2O=4.35%, P_2O_5=0.08%) with H_2O/O contents adjusted through *T*-H_2O (O) diagrams, normalized on the basis of mole percents as: SiO_2=66.35%, TiO_2=0.80%, Al_2O_3=13.11%, FeO=6.50%, MgO=5.95%, CaO=0.17%, Na_2O=0.53%, K_2O=3.02%, H_2O=3.40%, O=0.17%. (b) Effective bulk-rock compositions integrated the lost melt: SiO_2=65.60%, TiO_2=0.60%, Al_2O_3=11.64%, FeO=4.99%, MgO=4.49%, CaO=0.22%, Na_2O=0.82%, K_2O=3.30%, H_2O=8.21%, O=0.13%. The isopleths in the pseudosections are X_{Grs} in garnet, Ti in biotite, X_{Fe} in cordierite, Ab in K-feldspar and An in plagioclase

将其回算到实测全岩成分中，获得熔体迁移前的有效全岩成分．用该有效全岩成分计算的*P-T*视剖面图如图5(b)所示，其整体拓扑学关系与图5(a)有一定的相似性，但许多矿物相的稳定范围(如石榴子石、钛铁矿、金红石和熔体)有较大变化．其中，以金红石和钛铁矿共生为特征的包裹体矿物组合域显示了更小的温压范围．结合包裹体黑云母Ti的最大值和石榴子石核部X_{Grs}值，限定压力峰期阶段的温压条件为~0.95 GPa/800°C.

3.3 锆石年代学

锆石阴极发光(cathodoluminescene，CL)图像的拍摄和激光剥蚀电感耦合等离子体质谱仪(laser ablation inductively coupled plasma mass spectrometry, LA-ICP-MS)U-Pb定年测试分析在北京锆年领航科技有限公司完成．锆石定年分析仪器为AnlyitikJena PQMS Elite ICP-MS以及与之配套的ESI NWR 193 nm准分子激光剥蚀系统．激光剥蚀束斑直径为30 μm，频率为5 Hz，能量密度约为2.0 J/cm^2，载气为He．采用单点剥蚀的方式进行LA-ICP-MS激光剥蚀采样，测试前先用锆石标样GJ-1进行仪器调试，使之达到最优状态．锆石U-Pb定年以标样GJ-1为外标，微量元素含量利用SRM 610为外标、Si为内标的方法进行定量计算．测试过程中，每测定10个样品前后重复测定两个锆石标样GJ-1对样品进行校正，并测试一个锆石91500，观察仪器的状态以保证测试的精确度．数据处理采用ICPMSData-Cal程序[46]，同位素比值及年龄误差均为2σ．锆石年龄谐和图与加权平均年龄图等采用Isoplot/Ex 4.15进行绘制.

在CL图像(图6(a))上，高州泥质麻粒岩样品的锆石多为自形、半自形柱状或椭圆状，颗粒长径为100~150 μm．部分锆石具有明显的核-边结构，核部保留振荡环带，显示岩浆锆石的特征[47]，可能代表碎屑锆石残留；边部切割核部锆石的振荡环带，呈重结晶边围绕核部生长，显示斑杂状分带、弱分带或无分带，属于较为典型的变质重结晶特征[48]．其余锆石不显示核-边结构，环带特征和亮度均与前述具核-边结构锆石的变质边一致，应代表变质新生锆石[48]．本文对28个测试点进行了分析，包括核部碎屑锆石3个，变质边和变质新生锆石25个，数据结果见表S1和图6(b)．3个锆石核的年龄较老且存在一定跨度，$^{206}Pb/^{238}U$表观年龄分别为564±7.3、545±9和485±10 Ma，这些年龄与前人在高州地区获得的变质沉积岩碎屑年龄一致[36]．变质锆石的年龄相对集中，基本都落于谐和线上，25个测点获得441±1.4 Ma的谐和年龄，$^{206}Pb/^{238}U$加权平均年龄也为441±1.4 Ma(图6(b))．变质锆石的Th/U比值为0.15~0.41(表S1)．传统上认为，变质锆石的Th/U比值一般应低于0.10[48]，但变质锆石中的Th和U含量很容易受到变质流体或熔体的改造[49]，因此Th/U比值并不是判定锆石成因的绝对标准[50,51]．研究发现，高级变质岩石(如麻粒岩)的变质锆石很可能具有高的Th/U比值，有时这一比值可达10[48].

锆石变质边和变质新生锆石的稀土总量较高，稀土总量ΣREE=865~2105 μg/g，轻重稀土分馏较大，$(Nd/Yb)_N$<0.002，$(Gd/Yb)_N$=0.028~0.054，总体表现为轻稀土亏损、重稀土富集的左倾配分模式(图6(c))，与典型的跟熔体平衡的变质-深熔锆石的稀土元素配分模式较为相似[48]．重稀土富集可能是在岩石退变质过程中由石榴子石分解、熔体结晶所引起[50]．δEu<0.08，显示明显的Eu负异常，暗示这些变质锆石的生长过程可能与斜长石平衡[50]．锆石碎屑核部也显示重稀土富集的左倾配分模式，个别测点的稀土总量较低(图6(c))．为了限定变质锆石年龄所对应的变质阶段，本文利用Ferry和Watson[53]校正的锆石Ti温度计计算了变质锆石的结晶温度．考虑到高州泥质麻粒岩样品中存在石英和金红石(图6(b))，因此假设SiO_2和TiO_2的活度均为1[53]．样品变质锆石的Ti含量为5.5~11.5 μg/g(表S1)，获得锆石结晶温度为693~759°C，平均值为725±35°C(2σ)，与岩石温度峰期后冷却至固相线附近的温度接近(图5(a))．在现有的测试精度范围内，变质年龄与结晶温度之间并无明显的协变关系(图6(d))，推测变质锆石在约440 Ma时快速生长.

4 讨论与结论

4.1 高州泥质麻粒岩变质*P-T-t*演化

根据岩相学观察和相平衡模拟结果，高州泥质麻粒岩经历了包含3个变质阶段的顺时针型*P-T*演化：压力峰期阶段、温度峰期阶段和晚期退变质阶段．压力峰期阶段主要根据石榴子石的包裹体矿物组合(Grt+Ksp+Bt+Sil+Qz+Rt+Ilm+(L))限定，金红石与钛铁矿的共存表明压力位于0.75 GPa以上(图5(a))或0.90 GPa以上(图5(b))．利用熔体回算后的全岩成分计算相图，再结合包裹体黑云母的Ti含量和石榴子石核部X_{Grs}值，获得

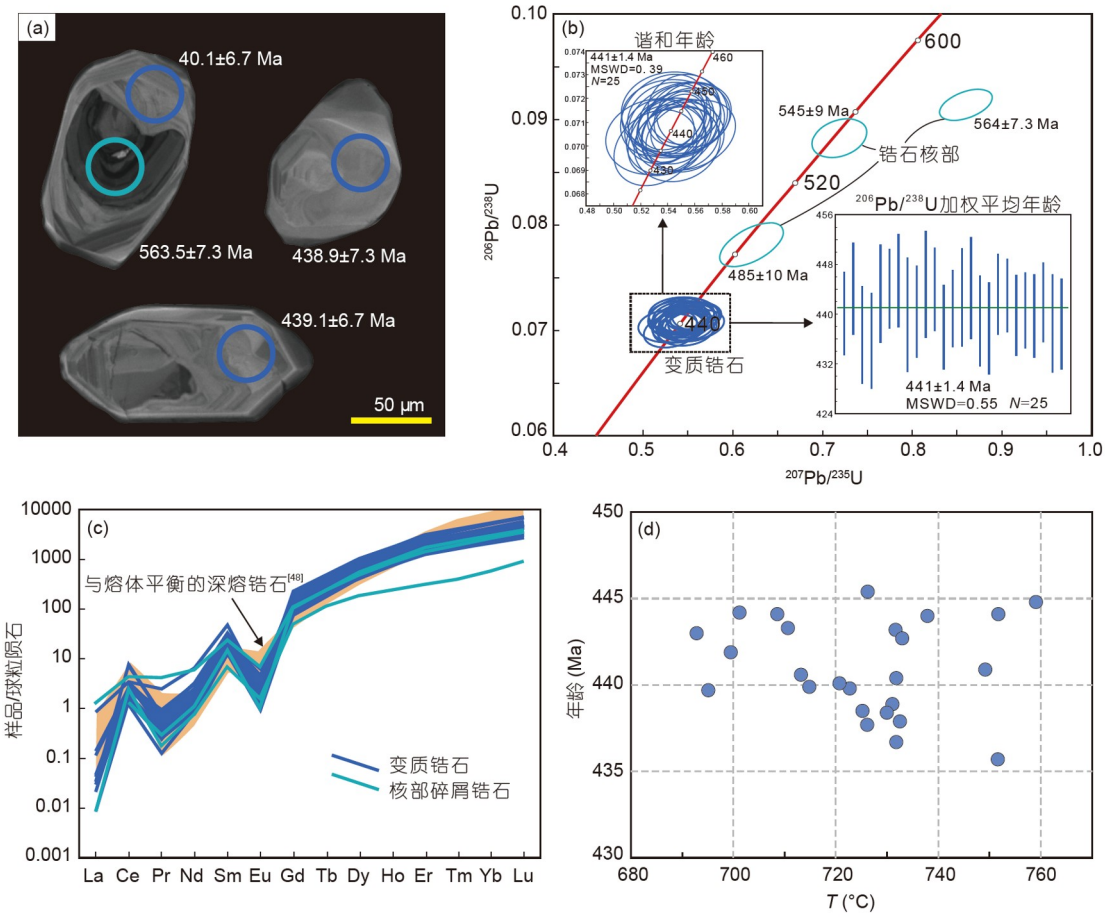

图 6 高州泥质麻粒岩锆石年代学结果. (a) 锆石CL图像; (b) 锆石U-Pb年龄谐和图; (c) 锆石稀土元素球粒陨石标准化图, 球粒陨石值据文献[52]; (d) 变质锆石年龄与结晶温度协变图

Figure 6 Zircon geochronology of pelitic granulite from Gaozhou. (a) CL images of zircons; (b) concordia diagram showing U-Pb analyses of zircons; (c) chondrite-normalized rare earth element (REE) patterns of zircons (chondrite data after Ref. [52]); (d) covariant relation of ages and crystallization temperatures of metamorphic zircons

压力峰期阶段的*P-T*条件为~0.95 GPa/ 800°C(图5(b)), 对应的视地热梯度为~850°C/GPa, 属于中压相系范围(图7). 这一压力峰期条件比Li等人[18]在高州半泥质-泥质麻粒岩中获得的压力峰期条件(0.70~0.80 GPa和730~780°C)稍高, 可能与在早前的样品中没有发现金红石有关. 温度峰期阶段由基质矿物组合(Grt+Crd+Ksp+Bt+Sil+Qz+Ilm+(L))限定, 结合基质黑云母Ti值和基质钾长石的Ab值, 得到了0.57~0.69 GPa/815~865°C的温压条件, 与前人在高州各类麻粒岩中获得的温度峰期结果基本一致[18,19,37].

华南早古生代变质作用的研究主要集中于华夏地块. 本文的相平衡模拟结果表明, 高州泥质麻粒岩与华夏地块其他地区的很多早古生代变质记录相似, 压力峰期阶段位于中压相系范围, 压力峰期阶段到温度峰期阶段以降压伴随一定程度的升温为特征, 温度峰期之后以降温降压为主(图7(a)). 上述变质*P-T*轨迹可以较好地反映岩石从加厚地壳深处抬升折返的过程, 系造山后重力均衡作用、剥蚀作用或其他构造因素共同影响的结果[60~62]. 在折返过程中, 可能还有岩浆作用提供外来热量[34], 岩石从压力峰期到温度峰期的升温或许与此有关, 研究区也发育很多同时代的花岗岩[10,36,38]. 岩石所记录的~0.95 GPa的最高压力表明, 岩石曾从地壳表层埋深进入30~35 km的深度, 但由于麻粒岩相高温阶段基本将岩石更早的矿物学记录抹去, 岩石的早期进变质过程已难以获得.

高州泥质麻粒岩样品的锆石U-Pb定年得到441±1.4 Ma的变质年龄(图6(b)). 这些变质锆石具有稀土总量高、轻重稀土分馏大的特点, 在球粒陨石标准

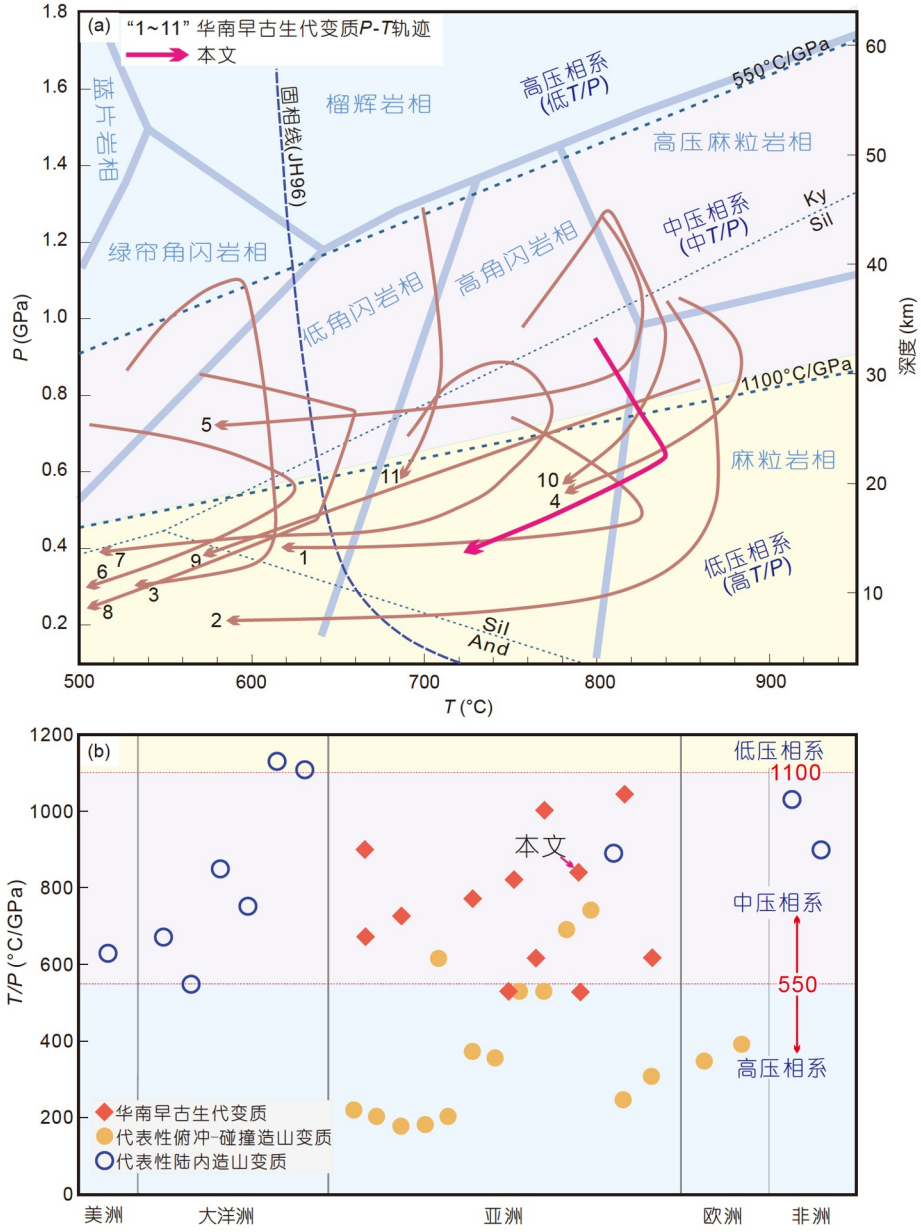

图 7 华南早古生代变质*P-T*轨迹综合图(a)以及华南早古生代变质、代表性陆内造山变质和俯冲-碰撞造山变质压力峰期阶段*T*/*P*点阵图(b). 固相线(JH96)为Qz-Ab-Or-H_2O体系下的饱和水固相线, 引自文献[54]. 变质相分界与变质相系范围引自文献[55], 蓝晶石/矽线石/红柱石转变线由THERMOCALC计算. 华南早古生代变质作用数据来源: “1”, 文献[18]; “2”, 文献[16]; “3”, 文献[56]; “4”, 文献[15]; “5”, 文献[57]; “6”, 文献[58]; “7”, 文献[59]; “8”, 文献[7]; “9”, 文献[12]; “10”, 文献[22]; “11”, 文献[14]. 代表性陆内造山变质和俯冲-碰撞造山变质的数据来源见表S2

Figure 7 Summarized early Paleozoic metamorphic *P-T* paths from South China (a) and metamorphic thermobaric ratios (*T*/*P*) for early Paleozoic metamorphism in South China, typical intraplate orogens and typical subduction-to-collision orogens (b). The solidus (JH96) is the H_2O-saturated solidus in the system Qz-Ab-Or-H_2O from Ref. [54]. Boundaries of metamorphic facies and metamorphic facies series are cited from Ref. [55]. The kyanite/sillimanite/andalusite transition lines were calculated by THERMOCALC. Data sources for early Paleozoic metamorphism in South China: “1”, Ref. [18]; “2”, Ref. [16]; “3”, Ref. [56]; “4”, Ref. [15]; “5”, Ref. [57]; “6”, Ref. [58]; “7”, Ref. [59]; “8”, Ref. [7]; “9”, Ref. [12]; “10”, Ref. [22]; “11”, Ref. [14]. Data sources for metamorphism of typical intraplate orogens and typical subduction-to-collision orogens are listed in Table S2

化的稀土配分图中显示左倾配分模式(图6(c)); 锆石Ti温度计的计算得出了693~759°C(平均值为725±35°C)的结晶温度(图6(d)). 本文将~441 Ma解释为岩石的退变质冷却时间, 主要基于以下4点思考: (1) 变质锆石的结晶温度低于岩石的压力峰期阶段和温度峰期阶段的温度条件, 而与岩石的固相线温度相近(图5(a)); (2) 变

质锆石的重稀土富集，稀土配分模式和那些与熔体平衡的锆石很类似[48]，暗示变质锆石生长时可能存在石榴子石的分解并伴随熔体的结晶[50]; (3) 变质锆石具有明显的Eu负异常, 指示与斜长石平衡共生[50], 岩相学观察和相平衡模拟表明，斜长石主要生长于岩石的晚期退变质阶段; (4) 发生了部分熔融的高级变质岩石，其锆石在进变质过程中容易被消耗-溶解进入熔体[63,64], 而在退变质冷却过程中从熔体中结晶出来并记录比实际峰期阶段更晚的年龄[65,66].

华夏地块已有的锆石/独居石U-Pb定年、石榴子石Lu-Hf定年和角闪石/云母^{40}Ar-^{39}Ar定年数据(表S3)表明, 早古生代变质事件主要发生在460~400 Ma. 在华夏地块北部的周潭地区，Zhao等人[67]识别出两阶段变质作用，其中挤压背景下的进变质阶段发生在460~450 Ma，而伸展背景下的高地热梯度变质阶段发生在~430 Ma; 同样地处华夏地块北部的龙游地区，进变质到峰期阶段的年龄主要为460~445 Ma[7,14,20,68]. Li等人[7]和Huang等人[69]总结了华夏地块中部武夷地区麻粒岩的变质年龄，认为这些岩石从进变质到峰期变质的时间为460~440 Ma，之后经历了445~420 Ma的深熔和接续的退变质冷却. 我们近期也对华夏地块北部的变质年龄开展了研究，发现不同区域的峰期变质年龄存在一定的差异，但基本都在450~435 Ma从进变质/峰期阶段(造山挤压增厚)向退变质/冷却阶段(造山后抬升)转变. 华夏地块西南部云开地体的变质年龄主要为446~428 Ma(表S3)，暂无老于450 Ma的变质年龄记录. 如果根据高州泥质麻粒岩样品的定年结果推测，进变质到麻粒岩相峰期阶段应早于441 Ma，很可能与华夏地块中北部一致.

4.2 构造意义

变质作用研究与热演化分析对于理解造山带构造过程很有意义[60,70]. 华南现有的早古生代变质*P*-*T*轨迹(图7(a))均为顺时针样式，部分岩石的峰期压力超过1 GPa，已属于常规语境下的“高压变质”范围. 但如果从更能反映构造意义的温度/压力(*T*/*P*)比值上看，这些变质岩石的压力峰期阶段主体仍位于中压相系，没有确凿的高压相系蓝片岩相或榴辉岩相变质证据. Cawood等人[71]将全球造山带分为增生型、碰撞型和陆内型3种基本类型. 传统上认为，中压相系变质作用是汇聚板块碰撞造山过程中十分常见的变质样式[34,60,70]. 但越来越多的证据表明，中压相系变质作用的形成环境并不单一, 在陆内造山的背景下也很常见, 国际上报道了很多相关的研究实例(图7(b)，如澳大利亚新元古代Peterman造山带和早古生代Alice Springs造山带、印度Bastar克拉通和Eastern Ghats Belt之间的剪切带早古生代造山作用、美洲的新元古代Central Ribeira Belt和南非的Limpopo杂岩古元古代造山运动[23,72~75]. Raimondo等人[23]、Gorczyk和Vogt[24]基于野外构造观测、变质作用分析和岩石热动力学模拟指出，陆内造山带在几何形态、地壳的缩短和增厚、山脉的隆升和折返以及热力学状态等方面与汇聚板块的碰撞造山带非常相似, 中压相系变质同样可以出现在陆内造山带中. 对于陆内造山的应力来源，目前认为有两种可能: (1) 由板块边缘碰撞产生的水平应力远程传播至陆内[23,24]; (2) 地幔的区域垂向应力引起大陆块体深部热力学和流变学结构的变化[76]. 持华南早古生代属于陆内造山观点的学者，普遍接受板块边界碰撞导致应力侧向传播的远程效应[1,5~8,11,20,29,69].

客观来说，蛇绿岩组合和弧相关岩石的缺失不能完全否定大陆碰撞模式，在部分典型的陆-陆碰撞造山带中也没有发现这些岩石组合，如大别-苏鲁造山带和西阿尔卑斯造山带[3,13,18]. 但需要指出的是，在变质作用方面，大别-苏鲁造山带和西阿尔卑斯造山带除了存在中压相系变质作用，还具有大量高压相系变质记录，出露很多经历过高压-超高压变质的蓝片岩、榴辉岩、大理岩和副片麻岩[77~80]. 华南陆块是否存在早古生代蛇绿岩组合和弧岩浆岩系列尚没有定论，其早古生代变质作用也与典型俯冲-碰撞造山带中既有中压相系变质又发育大量高压相系变质岩石的现象不完全相似(图7(b)). 因此, 就目前掌握的变质作用数据和其他地质资料分析, 华南陆块内部发育早古生代变质-岩浆-变形作用的构造域很可能并不是发生俯冲-碰撞的“第一现场”，引起该期构造热事件的应力来源于彼时华南的陆缘. 岩浆作用、变质作用、古生物学、沉积物源和古地磁证据表明，华南在早古生代时期应位于冈瓦纳大陆北缘，与澳大利亚-印度板块或Sibumasu板块相邻[19,81,82]. 有学者推测, 澳大利亚-印度板块与华南板块在早古生代沿着冈瓦纳大陆北缘拼合，所产生的远程效应导致华南内部发生变形、变质和大规模地壳重熔型岩浆活动[81]. 另外一些学者则认为, 华南北侧秦岭地区的板块汇聚、南侧越南中部Khmer陆块沿Tam Ky-Phuoc Son缝合带朝华南陆块的碰撞产生了远程应力[29,83,84].

致谢 感谢中山大学王岳军教授邀请和鼓励撰写此文, 感谢主编、评审专家的建议和帮助. 谨以此文庆贺中山大学地质学科百年华诞.

参考文献

1 Zhang C L, Santosh M, Zhu Q B, et al. The Gondwana connection of South China: Evidence from monazite and zircon geochronology in the Cathaysia Block. Gondwana Res, 2015, 28: 1137–1151

2 Wang Y, Wu C, Zhang A, et al. Kwangsian and Indosinian reworking of the eastern South China Block: Constraints on zircon U-Pb geochronology and metamorphism of amphibolites and granulites. Lithos, 2012, 150: 227–242

3 Zhao G, Cawood P A. Precambrian geology of China. Precambrian Res, 2012, 222-223: 13–54

4 Lin S, Xing G, Davis D W, et al. Appalachian-style multi-terrane Wilson cycle model for the assembly of South China. Geology, 2018, 46: 319–322

5 Ren J S. On the geotectonics of southern China (in Chinese). Acta Geol Sin, 1990, 4: 275–289 [任纪舜. 论中国南部的大地构造. 地质学报, 1990, 4: 275–289]

6 Shu L S. An analysis of principal features of tectonic evolution in South China Block (in Chinese). Geol Bull China, 2012, 31: 1035–1053 [舒良树. 华南构造演化的基本特征. 地质通报, 2012, 31: 1035–1053]

7 Li Z X, Li X H, Wartho J A, et al. Magmatic and metamorphic events during the early Paleozoic Wuyi-Yunkai orogeny, southeastern South China: New age constraints and pressure-temperature conditions. Geol Soc Am Bull, 2010, 122: 772–793

8 Zhang G W, Guo A L, Wang Y J, et al. Tectonics of South China continent and its implications. Sci China Earth Sci, 2013, 56: 1804–1828 [张国伟, 郭安林, 王岳军, 等. 中国华南大陆构造与问题. 中国科学: 地球科学, 2013, 43: 1553–1582]

9 Zheng Y F, Xiao W J, Zhao G. Introduction to tectonics of China. Gondwana Res, 2013, 23: 1189–1206

10 Huang X L, Yu Y. Geodynamics and origin of the early Paleozoic diachronous magmatism in South China (in Chinese). Geotecton Metall, 2022, 46: 435–454 [黄小龙, 于洋. 华南早古生代穿时岩浆活动成因与驱动机制. 大地构造与成矿学, 2022, 46: 435–454]

11 Shu L, Wang B, Cawood P A, et al. Early Paleozoic and Early Mesozoic intraplate tectonic and magmatic events in the Cathaysia Block, South China. Tectonics, 2015, 34: 1600–1621

12 Zhao L, Zhai M, Zhou X, et al. Thermal gradient and geochronology of a Paleozoic high-grade terrane in the northeastern Cathaysia block, South China. Tectonophysics, 2016, 691: 311–327

13 Chen X Y, Tong L X, Zhang C L, et al. Retrograde garnet amphibolite from eclogite of the Zhejiang Longyou area: New evidence of the Caledonian orogenic event in the Cathaysia block (in Chinese). Chin Sci Bull, 2015, 60: 1207–1217 [陈相艳, 仝来喜, 张传林, 等. 浙江龙游石榴石角闪岩(退变榴辉岩): 华夏加里东期碰撞造山事件的新证据. 科学通报, 2015, 60: 1207–1217]

14 Tong L, Li C, Liu Z, et al. First report of phengites in the Longyou paragneiss in the northern Early Paleozoic Wuyi-Yunkai orogen, South China: *P-T* conditions, zircon U-Pb ages and tectonic implications. J Asian Earth Sci, 2021, 214: 104754

15 Yu J F, Lou F S, Wang L J, et al. The geological significance of a Paleozoic mafic granulite found in the Yiyang area of northeastern Jiangxi Province (in Chinese). Chin Sci Bull (Chin Ver), 2014, 59: 3508–3516 [于津海, 楼法生, 王丽娟, 等. 赣东北弋阳早古生代麻粒岩的发现及其地质意义. 科学通报, 2014, 59: 3508–3516]

16 Yu J H, Zhou X M, Zhao L, et al. Discovery and implications of granulite facies metamorphic rocks in the eastern Nanling, China (in Chinese). Acta Petrol Sin, 2003, 19: 461–467 [于津海, 周新民, 赵蕾, 等. 南岭东段麻粒岩相变质岩的发现及其地质意义. 岩石学报, 2003, 19: 461–467]

17 Yu J H, Wang L J, Wei Z Y, et al. Phanerozoic metamorphic episodes and characteristics of Cathaysia Block (in Chinese). Geol J China Univ, 2007, 13: 474–483 [于津海, 王丽娟, 魏震洋, 等. 华夏地块显生宙的变质作用期次和特征. 高校地质学报, 2007, 13: 474–483]

18 Li C, Tong L, Liu Z, et al. *P-T* paths and U-Pb ages of pelitic and semi-pelitic granulites in the Yunkai massif and implication for the tectonic evolution of the Wuyi-Yunkai orogen, South China. J Asian Earth Sci, 2022, 224: 105010

19 Li C, Tong L X, Huang X L, et al. Metamorphic *P-T* history of calc-silicate granulites at Gaozhou in the Yunkai Massif, western Guangdong and its tectonic implications (in Chinese). Geotecton Metall, 2020, 44: 1172–1189 [李超, 仝来喜, 黄小龙, 等. 粤西云开地块高州钙硅酸盐麻粒岩的变质*P-T*历史及其构造意义. 大地构造与成矿学, 2020, 44, 1172–1189]

20 Wang J Q, Shu L S, Yu J H. From the Neoproterozoic mafic rock to the Silurian high-grade metamorphic rock: Evidence from zircon U-Pb geochronological, bulk-rock geochemical and mineral EPMA studies of Longyou garnet amphibolite in SE China. J Asian Earth Sci, 2017, 141: 7–23

21 Cheng H, Bloch E M, Moulas E, et al. Reconciliation of discrepant U-Pb, Lu-Hf, Sm-Nd, Ar-Ar and U-Th/He dates in an amphibolite from the Cathaysia Block in Southern China. Contrib Mineral Petrol, 2020, 175: 4

22 Qian J, Yin C, Zhang J, et al. Early Paleozoic high-temperature metamorphism of garnet amphibolite in the Longyou area, Cathaysia Block of South China: *P-T* path and tectonic implications. J Asian Earth Sci, 2021, 213: 104744

23 Raimondo T, Hand M, Collins W J. Compressional intracontinental orogens: Ancient and modern perspectives. Earth-Sci Rev, 2014, 130: 128–153

24 Gorczyk W, Vogt K. Tectonics and melting in intra-continental settings. Gondwana Res, 2015, 27: 196–208

25 Varga J, Raimondo T, Morrissey L, et al. Pressure-temperature-time constraints on gneiss dome formation in an intracontinental orogen. J Metamorph Geol, 2022, 40: 457–488

26 Peng S B, Liu S F, Lin M S, et al. Early Paleozoic subduction in Cathaysia (I): New evidence from Nuodong ophiolite (in Chinese). Earth Sci, 2016, 41: 765–778 [彭松柏, 刘松峰, 林木森, 等. 华夏早古生代俯冲作用(Ⅰ): 来自糯垌蛇绿岩的新证据. 地球科学, 2016, 41: 765–778]

27 Liu S, Peng S, Kusky T, et al. Origin and tectonic implications of an Early Paleozoic (460–440 Ma) subduction-accretion shear zone in the northwestern Yunkai Domain, South China. Lithos, 2018, 322: 104–128

28 Yu J H, Shu L S. Is the garnet amphibolite in the Longyou a retrograded eclogite (in Chinese)? Chin Sci Bull, 2016, 61: 556–560 [于津海, 舒良树. 龙游石榴石角闪岩是退变榴辉岩吗? 科学通报, 2016, 61: 556–560]

29 Shu L, Yao J, Wang B, et al. Neoproterozoic plate tectonic process and Phanerozoic geodynamic evolution of the South China Block. Earth-Sci Rev, 2021, 216: 103596

30 Li L, Lin S, Xing G, et al. Identification of ca. 520 Ma mid-ocean-ridge-type ophiolite suite in the inner Cathaysia block, South China: Evidence from shearing-type oceanic plagiogranite. GSA Bull, 2022, 134: 1701–1720

31 Zhao J H, Yang T, Wang W. Orogenic belt resulting from ocean-continent collision. Geology, 2022, 50: 1266–1269

32 Kun Z, Qingtian L, Zhao J, et al. Magnetotelluric evidence for the multi-microcontinental composition of eastern South China and its tectonic evolution. Sci Rep, 2020, 10: 13105

33 Wang L J, Lin S F, Xiao W J. Yangtze and Cathaysia blocks of South China: Their separate positions in Gondwana until early Paleozoic juxtaposition. Geology, 2023, 51: 723–727

34 Harley S L. The origins of granulites: A metamorphic perspective. Geol Mag, 1989, 126: 215–247

35 Warr L N. IMA-CNMNC approved mineral symbols. MinMag, 2021, 85: 291–320

36 Ke X Z, Zhou D, Long W G, et al. Indosinian metamorphism and anatexis in Yunkai Massif: Evidences from zircon geochronology and Hf isotopes of migmatites and gneisses (in Chinese). Earth Sci, 2018, 43: 2249–2275 [柯贤忠, 周岱, 龙文国, 等. 云开地块印支期变质－深熔作用: 混合岩、片麻岩锆石U-Pb年代学和Hf同位素证据. 地球科学, 2018, 43: 2249–2275]

37 Chen B, Zhuang Y X. The petrology and petrogenesis of Yunlu charnockite and its granulite inclusion, west Guangdong, South China (in Chinese). Acta Petrol Sin, 1994, 10: 139–150 [陈斌, 庄育勋. 粤西云炉紫苏花岗岩及其麻粒岩包体的主要特点和成因讨论. 岩石学报, 1994, 10: 139–150]

38 Li C, Tong L X, Liu Z, et al. Genesis of the Gaozhou charnockite and its two types of garnets of Yunkai massif, South China: Evidence from petrology and zircon U-Pb geochronology (in Chinese). Acta Petrol Sin, 2020, 36: 871–892 [李超, 仝来喜, 刘兆, 等. 华南云开高州紫苏花岗岩及其两类石榴石的成因: 岩石学和锆石U-Pb年代学证据. 岩石学报, 2020, 36: 871–892]

39 Kohn M J, Spear F. Retrograde net transfer reaction insurance for pressure-temperature estimates. Geology, 2000, 28: 1127–1130

40 Holland T J B, Powell R. An improved and extended internally consistent thermodynamic dataset for phases of petrological interest, involving a new equation of state for solids. J Metamorph Geol, 2011, 29: 333–383

41 White R W, Powell R, Holland T J B, et al. New mineral activity-composition relations for thermodynamic calculations in metapelitic systems. J Metamorph Geol, 2014, 32: 261–286

42 Holland T, Powell R. Activity-composition relations for phases in petrological calculations: An asymmetric multicomponent formulation. Contrib Mineral Petrol, 2003, 145: 492–501

43 White R W, Powell R, Holland T J B, et al. The effect of TiO_2 and Fe_2O_3 on metapelitic assemblages at greenschist and amphibolite facies conditions: Mineral equilibria calculations in the system K_2O-FeO-MgO-Al_2O_3-SiO_2-H_2O-TiO_2-Fe_2O_3. J Metamorph Geol, 2000, 18: 497–511

44 White R W, Powell R, Clarke G L. The interpretation of reaction textures in Fe-rich metapelitic granulites of the Musgrave Block, central Australia: Constraints from mineral equilibria calculations in the system K_2O-FeO-MgO-Al_2O_3-SiO_2-H_2O-TiO_2-Fe_2O_3. J Metamorph Geol, 2002, 20: 41–55

45 Tian Z L, Zhang Z M, Dong X. Calculation of effective bulk composition and its application in metamorphic phase equilibria modeling (in Chinese). Acta Petrol Sin, 2020, 36: 2616–2630 [田作林, 张泽明, 董昕. 有效全岩成分的计算方法及其在变质相平衡模拟中的应用. 岩石学报, 2020, 36: 2616–2630]

46 Liu Y, Gao S, Hu Z, et al. Continental and oceanic crust recycling-induced melt-peridotite interactions in the Trans-North China Orogen: U-Pb dating, Hf isotopes and trace elements in zircons from mantle xenoliths. J Petrol, 2010, 51: 537–571

47 Corfu F. Atlas of zircon textures. Rev Mineral Geochem, 2003, 53: 469–500

48 Rubatto D. Zircon trace element geochemistry: Partitioning with garnet and the link between U-Pb ages and metamorphism. Chem Geol, 2002, 184: 123–138

49 Mojzsis S J, Harrison T M. Establishment of a 3.83-Ga magmatic age for the Akilia tonalite (southern West Greenland). Earth Planet Sci Lett, 2002, 202: 563–576

50 Wu Y B. Metamorphic zircon. Encycl Geol, 2020, 2: 584–596

51 Lu C, Qian J, Yin C, et al. Ultrahigh temperature metamorphism recorded in the Lüliang Complex, Trans-North China Orogen: *P-T-t* evolution and heating mechanism. Precambrian Res, 2022, 383: 106900

52 Sun S, McDonough W F. Chemical and isotopic systematics of oceanic basalts: Implications for mantle composition and processes. Geol Soc Lond Spec Publ, 1989, 42: 313–345

53 Ferry J M, Watson E B. New thermodynamic models and revised calibrations for the Ti-in-zircon and Zr-in-rutile thermometers. Contrib Mineral Petrol, 2007, 154: 429–437

54 Johannes W, Holtz F. Petrogenesis and Experimental Petrology of Granitic Rocks. Berlin: Springer-Verlag, 1996

55 Wei C J, Duan Z Z. Phase relations in metabasic rocks: Constraints from the results of experiments, phase modelling and ACF analysis. Geol Soc Lond Spec Publ, 2019, 474: 25–45

56 Zhao G. Tectonothermal evolution of the Mayuan Assemblage in the Cathaysia Block: Implications for Neoproterozoic collision-related assembly of the South China Craton. Am J Sci, 1999, 299: 309–339

57 Guo T D, Zheng C Q, Zhou X W, et al. Metamorphism evolution and geological significance of garnet pyroxenite in Songyang area of southwestern Zhejiang Province (in Chinese). Acta Petrol Sin, 2018, 34: 3627–3642 [郭腾达, 郑常青, 周喜文, 等. 浙西南松阳地区石榴辉石岩变质作用演化与地质意义. 岩石学报, 2018, 34: 3627–3642]

58 Zhao G C, Sun D Y. The studies of metamorphic stages and metamorphic *p-T-D* path of Chencai Group, southwestern Zhejiang Province (in Chinese). J Changchun Univ Earth Sci, 1994, 24: 246–253 [赵国春, 孙德有. 浙西南陈蔡群变质阶段划分及变质作用*p-T-D*轨迹研究. 长春地质学院学报, 1994, 24: 246–253]

59 Xiang H. Phanerozoic metamorphism of Precambrian metamorphic basement in southwestern Zhejiang (in Chinese). Master Dissertation. Wuhan: China University of Geosciences, 2008 [向华. 浙西南前寒武纪变质基底岩系显生宙变质作用研究. 硕士学位论文. 武汉: 中国地质大学, 2008]

60 Spear F S. Metamorphic Phase Equilibria and Pressure-Temperature-Time Paths. Washington DC: Mineralogical Society of America, 1993. 799

61 Wei C J. Granulite facies metamorphism and petrogenesis of granite (II): Quantitative modeling of the HT-UHT phase equilibria for metapelites and the petrogenesis of S-type granite (in Chinese). Acta Petrol Sin, 2016, 32: 1625–1643 [魏春景. 麻粒岩相变质作用与花岗岩成因-Ⅱ: 变质泥质岩高温-超高温变质相平衡与S型花岗岩成因的定量模拟. 岩石学报, 2016, 32: 1625–1643]

62 Qian J, Yin C, Zhang J, et al. High-pressure granulites in the Fuping Complex of the central North China Craton: Metamorphic *P-T-t* evolution and tectonic implications. J Asian Earth Sci, 2018, 154: 255–270

63 Kelsey D E, Powell R. Progress in linking accessory mineral growth and breakdown to major mineral evolution in metamorphic rocks: A thermodynamic approach in the Na_2O-CaO-K_2O-FeO-MgO-Al_2O_3-SiO_2-H_2O-TiO_2-ZrO_2 system. J Metamorph Geol, 2011, 29: 151–166

64 Zhang Y H, Wei C J, Tian W, et al. Reinterpretation of metamorphic age of the Hengshan Complex, North China Craton. Chin Sci Bull, 2013, 58: 4300–4307

65 Wei C, Qian J, Zhou X. Paleoproterozoic crustal evolution of the Hengshan-Wutai-Fuping region, North China Craton. Geosci Front, 2014, 5: 485–497

66 Qian J, Yin C, Li S, et al. Metamorphic *P-T-t* evolution of amphibolite in the north Hengshan terrane, North China Craton: Insights into the late Paleoproterozoic tectonic processes from initial collision to final exhumation. GSA Bull, 2021, 133: 2017–2030

67 Zhao L, Zhang R C, Zhai M G, et al. Major lithologies of the high-grade Zhoutan terrane within the Cathaysia Block and their tectonic implications for the Neoproterozoic-Paleozoic South China. Lithos, 2020, 372-373: 105664

68 Wang J G, Yu S Q, Hu Y H, et al. The discovery, petrology and geochronology of the retrograde eclogite in Jiangnan-Shaoxing suture zone (in Chinese). Geol China, 2014, 41: 1356–1363 [汪建国, 余盛强, 胡艳华, 等. 江山-绍兴结合带榴闪岩的发现及岩石学、年代学特征. 中国地质, 2014, 41: 1356–1363]

69 Huang D L, Wang X L, Xia X P, et al. Crustal anatexis recorded by zircon grains from early Paleozoic granitic rocks in Southeast China. Lithos, 2020, 370-371: 105598

70 Brown M, Johnson T. Secular change in metamorphism and the onset of global plate tectonics. Am Miner, 2018, 103: 181–196

71 Cawood P A, Kröner A, Collins W J, et al. Accretionary orogens through Earth history. Geol Soc Lond Spec Publ, 2009, 318: 1–36

72 Korhonen F J, Johnson S P, Wingate M T D, et al. Radiogenic heating and craton-margin plate stresses as drivers for intraplate orogeny. J Metamorph Geol, 2017, 35: 631–661

73 Meira V T, Garcia-Casco A, Hyppolito T, et al. Tectono-metamorphic evolution of the central Ribeira Belt, Brazil: A case of Late Neoproterozoic intracontinental orogeny and flow of partially molten deep crust during the assembly of West Gondwana. Tectonics, 2019, 38: 3182–3209

74 Padmaja J, Sarkar T, Dasgupta S, et al. High pressure granulite facies metamorphism at the interface of the Archean Bastar craton and the

Proterozoic Eastern Ghats Belt, India. Precambrian Res, 2021, 363: 106330
75 Basupi T O, Tsunogae T, Tsutsumi Y. Petrology and geochronology of sapphirine-bearing granulites from the Limpopo Complex in eastern Botswana: Implications for Palaeoproterozoic long-lived high-pressure/ultrahigh-temperature metamorphism and rapid exhumation. Geol J, 2022, 57: 4194–4215
76 Pysklywec R N, Beaumont C, Fullsack P. Modeling the behavior of the continental mantle lithosphere during plate convergence. Geology, 2000, 28: 655–658
77 Zhu Y F, Massonne H J, Men-Fan Zhu H J. Petrology of low-temperature, ultrahigh-pressure marbles and interlayered coesite eclogites near Sanqingge, Sulu terrane, eastern China. Mineral Mag, 2009, 73: 307–332
78 Liu P L, Wu Y, Chen Y, et al. UHP impure marbles from the Dabie Mountains: Metamorphic evolution and carbon cycling in continental subduction zones. Lithos, 2015, 212-215: 280–297
79 Malatesta C, Federico L, Crispini L, et al. Fluid-controlled deformation in blueschist-facies conditions: Plastic vs brittle behaviour in a brecciated mylonite (Voltri Massif, Western Alps, Italy). Geol Mag, 2018, 155: 335–355
80 Vanardois J, Roger F, Trap P, et al. Exhumation of deep continental crust in a transpressive regime: The example of Variscan eclogites from the Aiguilles-Rouges massif (Western Alps). J Metamorph Geol, 2022, 40: 1087–1120
81 Cawood P A, Zhao G, Yao J, et al. Reconstructing South China in Phanerozoic and Precambrian supercontinents. Earth-Sci Rev, 2018, 186: 173–194
82 Li S, Zhao S, Liu X, et al. Closure of the Proto-Tethys Ocean and Early Paleozoic amalgamation of microcontinental blocks in East Asia. Earth-Sci Rev, 2018, 186: 37–75
83 Gardner C J, Graham I T, Belousova E, et al. Evidence for Ordovician subduction-related magmatism in the Truong Son terrane, SE Laos: Implications for Gondwana evolution and porphyry Cu exploration potential in SE Asia. Gondwana Res, 2017, 44: 139–156
84 Faure M, Nguyen V V, Hoai L T T, et al. Early Paleozoic or Early-Middle Triassic collision between the South China and Indochina Blocks: The controversy resolved? Structural insights from the Kon Tum massif (Central Vietnam). J Asian Earth Sci, 2018, 166: 162–180

补充材料

图S1 高州泥质麻粒岩附近的片麻状S型花岗岩露头
图S2 高州泥质麻粒岩露头
图S3 高州泥质麻粒岩石榴子石含量统计图
图S4 沿高州泥质麻粒岩*P-T*轨迹模拟的矿物含量变化图
表S1 高州泥质麻粒岩LA-ICP-MS锆石U-Pb年代学结果
表S2 代表性陆内造山带、俯冲-碰撞造山带和华南早古生代变质温压比数据
表S3 华夏地块早古生代变质年龄

本文以上补充材料见网络版csb.scichina.com. 补充材料为作者提供的原始数据, 作者对其学术质量和内容负责.

Summary for “粤西高州泥质麻粒岩变质*P-T-t*演化及其对华南早古生代构造背景的指示”

Metamorphic *P-T-t* evolution of pelitic granulite from Gaozhou, western Guangdong Province and its implications for the Early Paleozoic tectonic setting in South China

Jiahui Qian[1*], Yongzhi Liang[1], Changqing Yin[1], Peng Gao[1], Jian Zhang[2] & Reziya Maimaiti[1]

[1] *Guangdong Provincial Key Laboratory of Mineral Resources & Geological Processes, School of Earth Sciences and Engineering, Sun Yat-sen University, Zhuhai 519080, China;*
[2] *Department of Earth Sciences, The University of Hong Kong, Hong Kong 999077, China*
* Corresponding author, E-mail: qianjh5@mail.sysu.edu.cn

The formation and evolution of the early Paleozoic tectono-thermal event in South China remains a hotly debated topic within the academic community. Studies of metamorphism can provide pivotal insight into this issue. In this contribution, detailed studies of petrography, mineral chemistry, phase equilibria modelling and zircon U-Pb geochronology have been carried out on pelitic granulite from Gaozhou, southwestern part of the Cathaysia Block, South China. This paper will compare the early Paleozoic metamorphic data in the Cathaysia block to the new data provided here in order to discuss tectonic setting in South China. The pelitic granulite contains three generations of mineral assemblage, namely the inclusion, matrix and retrograde mineral assemblages. The inclusion mineral assemblage consists of garnet core and the wrapped K-feldspar, biotite, sillimanite, quartz, rutile and ilmenite within garnet. *P-T* conditions of the inclusion mineral assemblage are ~0.95 GPa and 800°C (P_{max} stage), obtained by phase equilibria modelling using software THERMOCALC. The matrix mineral assemblage consists of garnet porphyroblast and the matrix-type cordierite, K-feldspar, biotite, quartz, sillimanite and ilmenite. Combined with the domain of matrix mineral assemblage in the pseudosection, the Ti content of matrix-type biotite and the Ab value of matrix-type K-feldspar, *P-T* conditions of the matrix mineral assemblage are defined to be 0.57−0.69 GPa and 815−865°C (T_{max} stage). The retrograde mineral assemblage is composed by late cordierite, K-feldspar, biotite, plagioclase, sillimanite, quartz and ilmenite. Mineral compositions and stabilities indicate that the retrograde metamorphism is characterized by cooling and decompression. Zircon U-Pb dating of the pelitic granulite yields a metamorphic age of 441±1.4 Ma. Ti-in-zircon thermometer applied for the metamorphic zircons gives crystallization temperatures of 693−759°C, which are consistent with the temperatures of the retrograde (cooling) metamorphic stage of the rock. Therefore, this metamorphic age is interpreted to represent the timing of retrograde metamorphism. After analysing the early Paleozoic metamorphic data collected from the Cathaysia block, it is concluded that the early Paleozoic metamorphism in South China matches with medium-pressure facies series and show clockwise *P-T* paths, without high-pressure facies series blueschist or eclogite being found yet. Medium-pressure facies series metamorphism can be formed both in continental collision orogens and intracontinental orogenic belts. However, those collision orogens are also featured by the presence of high- to ultrahigh-pressure blueschist and eclogite. The tectonic domains that underwent the early Paleozoic metamorphism, magmatism, and deformation are most likely not the locations of subduction-collision, based on current metamorphic data and other geological features (such as the lack of compelling ophiolites and arc-related magmatic rocks) in South China. The tectonic stress causing the early Paleozoic tectono-thermal event should come from the continental margin of South China at that time.

pelitic granulite, metamorphic *P-T-t* evolution, early Paleozoic, tectonic significance, South China

doi: 10.1360/TB-2023-0835